

Polarizing efficiency as a guide of grain growth and interstellar magnetic field properties

N.V. Voshchinnikov^{1*}, V.B. Il'in^{1,2,3} and H.K. Das⁴

¹*Sobolev Astronomical Institute, St. Petersburg University, Universitetskii prosp., 28, St. Petersburg 198504, Russia*

²*Main (Pulkovo) Astronomical Observatory, Pulkovskoe sh. 65, St. Petersburg 196140, Russia*

³*St. Petersburg State University of Aerospace Instrumentation, Bol. Morskaya 67, St. Petersburg 190000, Russia*

⁴*IUCAA, Post Bag 4, Ganeshkhind, Pune 411 007, India*

Accepted 2016 July 18; Received 2016 July 15; in original form 2015 November 21

ABSTRACT

We interpret the relation between the polarizing efficiency $P_{\max}/E(B - V)$ and the wavelength of the maximum polarization λ_{\max} observed for 17 objects (including 243 stars) separated into two groups: “dark clouds” and “open clusters”. The objects are assigned to one of the groups according to the distribution of the parameter λ_{\max} . We use the model of homogeneous silicate and carbonaceous spheroidal particles with the imperfect alignment and a time-evolving size distribution. The polarization is assumed to be mainly produced by large silicate particles with the sizes $r_V \gtrsim r_{V,\text{cut}}$. The models with the initial size distribution reproducing the average curve of the interstellar extinction fail to explain the values of $\lambda_{\max} \gtrsim 0.65 \mu\text{m}$ observed for several dark clouds. We assume that the grain size distribution is modified due to accretion and coagulation, according to the model of Hirashita & Voshchinnikov (2014). After including the evolutionary effects, λ_{\max} shifts to longer wavelengths on time-scales $\sim 20(n_{\text{H}}/10^3 \text{cm}^{-3})^{-1} \text{Myr}$ where n_{H} is the hydrogen density in molecular clouds where dust processing occurs. The ratio $P_{\max}/E(B - V)$ goes down dramatically when the size of polarizing grains grows. The variations of the degree and direction of particle orientation influence this ratio only moderately. We have also found that the aspect ratio of prolate grains does not affect significantly the polarizing efficiency. For oblate particles, the shape effect is stronger but in most cases the polarization curves produced are too narrow in comparison with the observed ones.

Key words: polarization — dust, extinction — galaxies: evolution — galaxies: ISM — ISM: clouds

1 INTRODUCTION

Non-spherical dust grains are responsible for the interstellar polarization phenomenon. The polarization becomes significant when interstellar grains are well aligned and have sizes comparable to the wavelength of the incident radiation. Alignment of dust particles can arise due to their specific magnetic properties giving them the ability to efficiently interact with the interstellar magnetic fields.

The interstellar linear polarization is characterized by the polarization degree P and the position angle θ_{E} or θ_{G} measured either in the equatorial or galactic coordinate system, respectively. The polarization degree usually tends to a maximum in the visual and gradually decreases to the ultraviolet and infrared. The wavelength dependence of polarization $P(\lambda)$ is described by an empirical formula suggested in Serkowski (1973) and now called Serkowski curve

$$P(\lambda)/P_{\max} = \exp[-K \ln^2(\lambda_{\max}/\lambda)]. \quad (1)$$

This formula has three parameters: P_{\max} is the maximum degree of polarization, λ_{\max} the wavelength corresponding to it, and K the coefficient characterizing the width of the Serkowski curve. The values of P_{\max} in the diffuse interstellar medium usually do not exceed 10%, and the average value of λ_{\max} is $0.55 \mu\text{m}$ (Serkowski et al. 1975). The parameter K is related to the half-width of the normalized polarization curve

$$W = \lambda_{\max}/\lambda_- - \lambda_{\max}/\lambda_+, \quad (2)$$

where λ_-, λ_+ are such that $P(\lambda_+) = P(\lambda_-) = P_{\max}/2$ and $\lambda_- < \lambda_{\max} < \lambda_+$. The relation between W and K is as follows:

$$W = \exp[(\ln 2/K)^{1/2}] - \exp[-(\ln 2/K)^{1/2}]. \quad (3)$$

Initially, the parameter K was chosen to be 1.15 (Serkowski 1973). Later, Whittet et al. (1992) found a dependence of K on λ_{\max} in the Milky Way

$$K = (1.66 \pm 0.09)\lambda_{\max} + (0.01 \pm 0.05), \quad (4)$$

where λ_{\max} is in microns.

The ratio of P_{\max} to the colour excess $E(B - V)$ or visual

* E-mail: n.voshchinnikov@spbu.ru

Table 1. Target objects.

N	Object	N_{stars}	l	b	D , pc	$\langle \lambda_{\text{max}} \rangle$, μm	$\left\langle \frac{P_{\text{max}}}{E(B-V)} \right\rangle$	$\theta_{0,G} \pm \sigma_{\theta_{0,G}}$	References
(1)	(2)	(3)	(4)	(5)	(6)	(7)	(8)	(9)	(10)
Dark clouds									
1	Taurus: cloud 1	31	174	-14	147	0.570 ± 0.049	6.01 ± 2.09	156.5 ± 13.1	[1,2,3]
2	Chamaeleon I	25	297	-15	196	0.594 ± 0.064	9.46 ± 2.53	101.3 ± 10.8	[4,5,6]
3	ρ Oph: cloud 1	10	353	+18	133	0.684 ± 0.110	3.85 ± 1.56	31.4 ± 14.4	[7,8,9,10]
4	cloud 2	20				0.659 ± 0.059	6.19 ± 3.21	98.3 ± 11.2	
5	R CrA: cloud A1	9	359	-18	148	0.758 ± 0.104	3.48 ± 1.62	132.0 ± 24.1	[4,5,11]
6	cloud A2	5				0.734 ± 0.080	2.21 ± 1.12	52.1 ± 14.3	
7	cloud B	5				0.690 ± 0.071	5.48 ± 2.57	153.4 ± 11.0	
8	CMa R1: cloud 1	5	225	-1	690	0.637 ± 0.030	4.80 ± 2.06	132.4 ± 13.0	[12]
9	cloud 2	6				0.593 ± 0.149	2.31 ± 1.06	75.7 ± 24.3	
Open clusters (and some dark clouds)									
10	Taurus: cloud 2	13	174	-14	147	0.556 ± 0.043	5.76 ± 1.61	26.1 ± 20.4	[2,3]
11	α Per	36	147	-6	213	0.543 ± 0.051	8.10 ± 2.63	86.7 ± 13.8	[13]
12	Musca	16	300	-9	171	0.577 ± 0.017	12.62 ± 2.98	102.9 ± 3.9	[4]
13	Southern Coalsack	14	301	-1	174	0.570 ± 0.040	6.31 ± 2.73	75.3 ± 17.4	[4]
14	NGC 654	6	129	-0	2410	0.555 ± 0.019	4.14 ± 0.71	87.3 ± 4.5	[14]
15	IC 1805	16	134	+1	2400	0.540 ± 0.031	5.70 ± 1.14	96.1 ± 5.0	[15]
16	NGC 6124	11	341	+6	563	0.574 ± 0.039	3.40 ± 0.84	54.0 ± 4.7	[16]
17	Cyg OB2	15	80	+1	1700	0.473 ± 0.073	2.07 ± 0.71	146.6 ± 26.2	[5,7]

References: [1] – Efimov 2009; [2] – Whittet et al. 2001; [3] – Hsu 1985; [4] – Andersson & Potter 2007; [5] – Whittet et al. 1992; [6] – McGregor et al. 1994; [7] – Martin et al. 1992; [8] – Wilking et al. 1982; [9] – Vrba et al. 1993; [10] – Snow et al. 2008; [11] – Vrba et al. 1981; [12] – Vrba et al. 1987; [13] – Coyne et al. 1979; [14] – Medhi et al. 2008; [15] – Medhi et al. 2007; [16] – Vergne et al. 2010.

extinction A_V is called the *polarizing efficiency*. There exists an empirical limit to this ratio (Serkowski et al. 1975)

$$\frac{P_{\text{max}}}{E(B-V)} \lesssim 9\%/\text{mag}. \quad (5)$$

or

$$\frac{P_{\text{max}}}{A_V} = \frac{P_{\text{max}}}{R_V E(B-V)} \lesssim 3\%/\text{mag}, \quad (6)$$

where R_V is the total to selective extinction ratio.

A qualitative explanation of the relation (4) between the width of the interstellar polarization curve and the position of its maximum is connected to the fact that dust grains grow in the accretion and coagulation processes, which leads to a narrowing of the particle size distribution (see, e.g., Whittet et al. 1992). A quantitative interpretation of the dependence $K(\lambda_{\text{max}})$ was suggested by Aannestad & Greenberg (1983) who considered cylindrical particles and by Voshchinnikov et al. (2013) and Voshchinnikov & Hirashita (2014) who used spheroidal grains.

However, all three parameters of the Serkowski curve have been determined for a limited number of stars (less than 200; Voshchinnikov & Hirashita 2014). This is because one needs to perform observations in more than four or even five bands (Whittet et al. 1992) to find the width of the polarization curve (parameter K) with a good accuracy. In contrast, the parameters P_{max} and λ_{max} can be determined with a sufficient accuracy when stars are observed just in three or four bands. Hence, there exists a significant number of lines of sight for which both the polarizing efficiency and the wavelength of maximum polarization have been estimated.

The polarizing efficiency in a given direction depends on the size of polarizing and non-polarizing grains, the particle shape and the degree and direction of grain alignment. In general, the dust grain characteristics and the magnetic field can vary along the

line of sight. As a basic model we use that of imperfectly aligned spheroidal particles in a regular magnetic field that was earlier applied to simultaneously analyse the interstellar extinction and polarization curves in a wide spectral range (Voshchinnikov & Das 2008; Das et al. 2010; Siebenmorgen et al. 2014). We consider the time evolution of the grain size distribution due to accretion and coagulation processes (Hirashita & Voshchinnikov 2014) and involved new optical constants of grain materials (Jones 2012; Jones et al. 2013). Voshchinnikov & Hirashita (2014, hereafter VH14) used such a model to investigate the relation between K and λ_{max} that are the parameters of the Serkowski curve which characterize its width and maximum position, respectively.

In this paper, we focus on interpretation of the observed dependencies of $P_{\text{max}}/E(B-V)$ on λ_{max} and show that the most important factor influencing these dependencies is the size of polarizing grains. The paper is organized as follows: Sections 2 and 3 give a description of the observational data and the model used, Section 4 presents results of our modelling of the polarizing efficiency and their discussion, and Section 5 contains the conclusions made.

2 OBSERVATIONAL DATA

We have collected available observational data on the polarizing efficiency $P_{\text{max}}/E(B-V)$ and the maximum polarization position λ_{max} from the literature. We started with a list of 160 stars with the known values of the parameter K considered in VH14. From the list, we selected stars closely located in the sky and with similar values of the polarization position angle. We extended these groups by including stars with the known values of P_{max} , λ_{max} , and $E(B-V)$ and excluded the stars with significant wavelength rotation of the position angle and large errors in observational data.

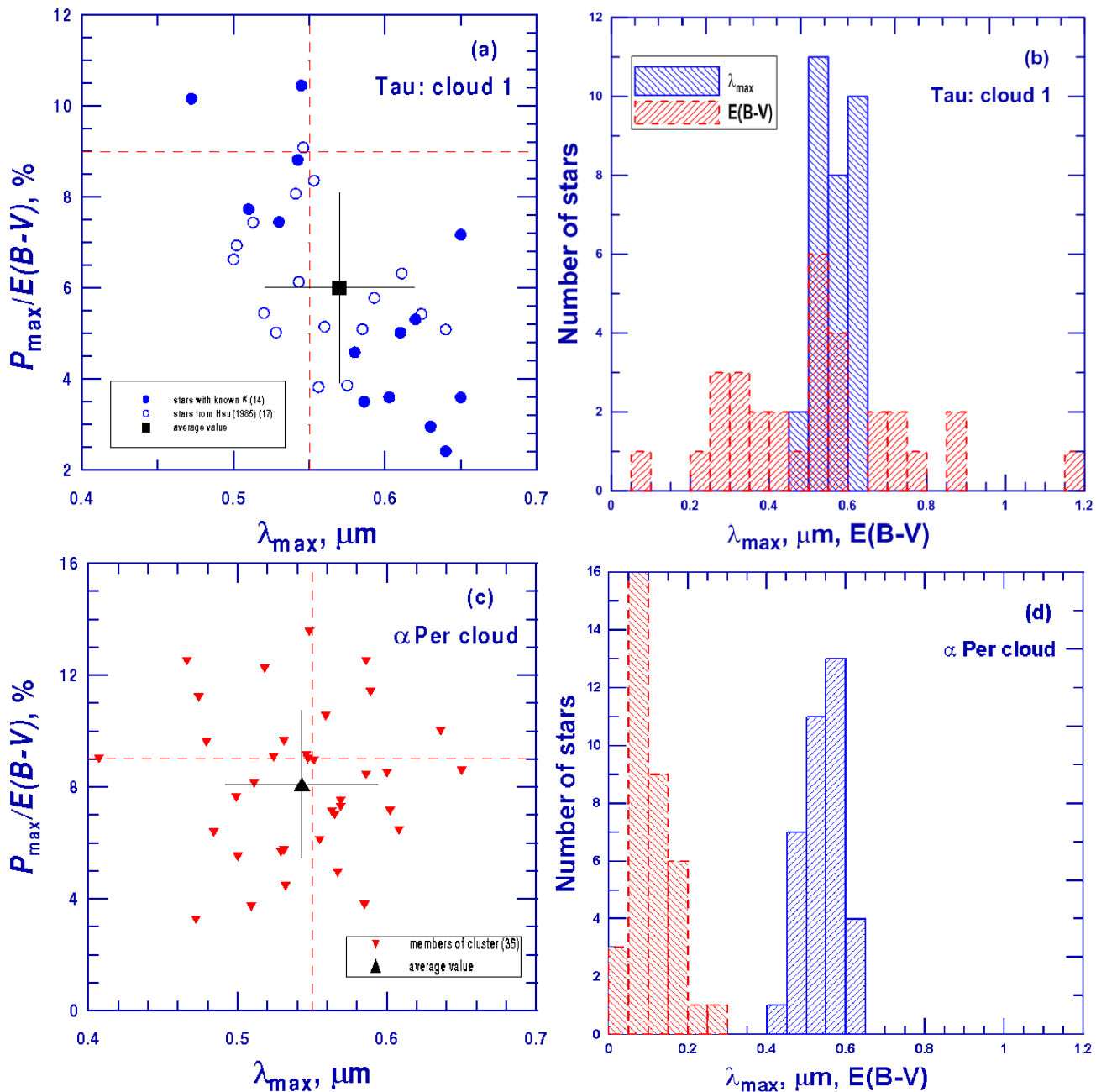


Figure 1. Polarizing efficiency $P_{\max}/E(B - V)$ versus the wavelength of maximum polarization λ_{\max} for dark cloud 1 in Taurus (a) and cluster α Per (c). The average values $\langle \frac{P_{\max}}{E(B-V)} \rangle$ are plotted with standard deviations. Vertical and horizontal dashed lines correspond to the mean interstellar value of $\lambda_{\max} = 0.55 \mu\text{m}$ and the upper limit of the polarizing efficiency given by equation (5). Panels (b) and (d) show the histograms of the distributions of λ_{\max} and $E(B - V)$ for Taurus cloud 1 and α Per cluster, respectively.

Moreover, we chose only the probable members of the stellar clusters.

Our final list contains 243 stars associated with 17 objects that are either a dark cloud or a stellar cluster. We separate the objects into two groups according to the patterns seen on their dependence of $P_{\max}/E(B - V)$ on λ_{\max} (see Fig. 1). All the objects are listed in Table 1 that includes the number of stars considered, the coordinates and distances to the objects, the average values of the wavelength of maximum polarization with the deviations. The last column gives the sources of the observational data. We took the distances to the objects from Knude (2010) and the papers cited in

Table 1. Most of the objects are not very distant and either belong to the Gould Belt or are close to it. The exceptions are NGC 654 and IC 1805 located in the direction of the anti-center of the Galaxy where the interstellar medium is transparent up to large distances (Lallement et al. 2014).

For the clusters, polarization of their stars is mainly caused by dust in the diffuse medium in the line of sight. On the plots we see a cloud of points around some mean polarization efficiency, with λ_{\max} being usually in the interval $0.5 - 0.6 \mu\text{m}$ (see Fig. 1c,d). The clusters produce what we call the open cluster pattern.

For the dark clouds, when a part of the stars with measured

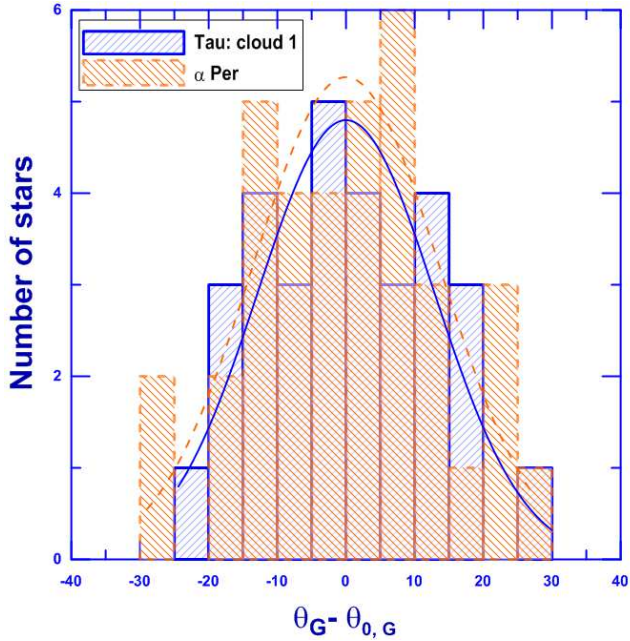


Figure 2. Number distribution of the position angles around the mean value $\theta_{0,G}$ for the dark cloud 1 in Taurus and cluster α Per. Curves show the Gaussian fits of the observational data.

polarization are seen through outer layers of the cloud, we meet another pattern called the dark cloud pattern. The stars observed mainly through diffuse medium, i.e. foreground, aside, distant stars, produce again nearly the open cluster pattern, but the stars seen through the dark cloud sometimes add a trend: the larger λ_{\max} , the smaller the polarization efficiency (see Fig. 1a,b).

Obviously, when the part of stars seen through the dark cloud is very small, we approach the open cluster pattern, even though the stars are at different distances, while for the clusters the distances are nearly the same. This pattern is seen in our data for Taurus cloud 2, Musca cloud, and Southern Coalsack.

The way we associate the stars with the objects is to some extent arbitrary and is based on the data published in the papers listed in Table 1 (e.g., Vrba et al. 1981 set off the cloud A¹ and cloud B in the dark cloud R CrA). In Taurus, two groups of stars with a relatively uniform distribution of the position angles (cloud 1, $\theta_G = 145^\circ - 175^\circ$ and cloud 2, $\theta_G = 2^\circ - 40^\circ$) were described by Voshchinnikov (2012) on the basis of the initial analysis of Messenger et al. (1997). Stars in “clouds” are distributed around complexes of molecular clouds and partly are projected on them. In these cases, the interstellar extinction can differ significantly, in contrast to stars of “clusters” when it lies in a rather narrow range (cf. Figs. 1b and 1d). A negative correlation between $P_{\max}/E(B-V)$ and λ_{\max} for the dark cloud 1 in Taurus and a uniform distribution of data for α Per cluster are well seen in the figures. Note that neither such a correlation nor its absence is typical of the clouds and clusters. Probably, the correlation is formed by local conditions and is partly a result of observational selection.

Column (8) in Table 1 shows the average values of the polarizing efficiency derived from observations. These values do not take into account the depolarization effect due to spatial variations of the magnetic field \mathbf{B} . This effect can be

¹ Besides this, we distinguished clouds A1 and A2.

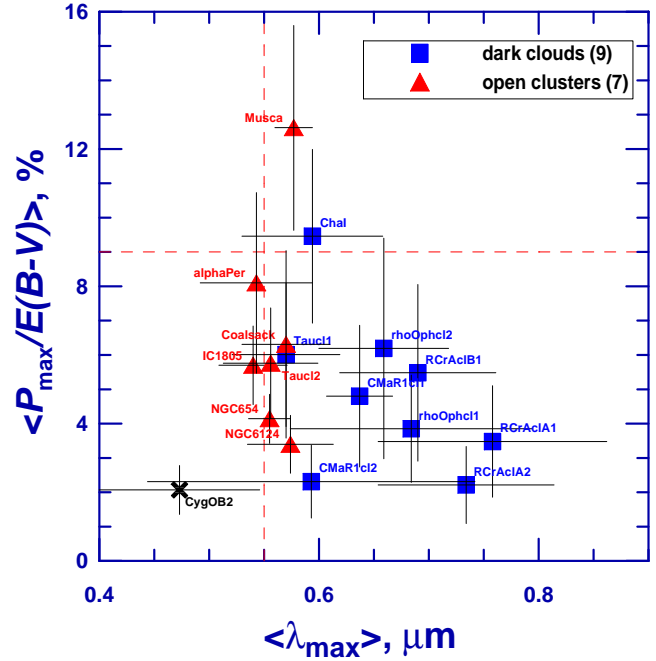


Figure 3. Average polarizing efficiency $\langle P_{\max}/E(B-V) \rangle$ versus the average wavelength of maximum polarization $\langle \lambda_{\max} \rangle$ for dark clouds (squares) and open clusters (triangles) in the Milky Way. Vertical and horizontal dashed lines correspond to the mean interstellar value of $\lambda_{\max} = 0.55 \mu\text{m}$ and the upper limit of the polarizing efficiency given by equation (5). The number of stars, coordinates of objects, sources of data, etc. are presented in Table 1.

found as the dispersion in directions of polarization angle. A similar approach has been applied to optical polarization (Myers & Goodman 1991; Jones et al. 1992) and submm polarization measured by *Planck* (Planck Collaboration Int. XXXII 2016; Planck Collaboration Int. XXXV 2016; Planck Collaboration Int. XLIV 2016; Guillet 2015).

Myers & Goodman (1991) studied the spatial patterns and distributions of the direction of the interstellar polarization for several clouds, clusters and complexes of clouds. They found that the number distributions often had a single local maximum with the dispersion of 0.2 – 0.5 radians and the clouds had a larger dispersion than the clusters. We calculate the mean value of the position angle $\theta_{0,G}$ and its dispersion $\sigma_{\theta_{0,G}}$ for our objects (see column 9 in Table 1). Figure 2 presents the number distribution of the position angle for the dark cloud 1 in Taurus and cluster α Per together with the Gaussian fits. Note that the dispersions $\sigma_{\theta_{0,G}}$ are very close to the widths of Gaussian curves ($13^\circ 1$ vs $12^\circ 9$ and $13^\circ 8$ vs $13^\circ 6$ for dark cloud 1 in Taurus and cluster α Per, respectively). Though we used the data different from those of Myers & Goodman (1991), the dispersions found for α Per and Cha I do not differ more than by 20%. For the regions in Ophiuchus and Taurus the difference is about 50% mainly because we considered separate clouds, while Myers & Goodman (1991) large complexes.

Figure 3 shows the average polarizing efficiency versus the average wavelength of maximum polarization for target objects. One clearly sees two patterns in distribution of the $\langle \lambda_{\max} \rangle$ values: for the open clusters and some clouds, the mean values of λ_{\max} are grouped around the average interstellar value equal to $0.55 \mu\text{m}$ with rather small deviations, while for most dark clouds, the values of $\langle \lambda_{\max} \rangle$ may be significantly larger than $0.55 \mu\text{m}$ and have a wider scattering. Note also that in two cases (Cha I and Musca) the

average polarizing efficiency exceeds the upper observational limit given by equation (5).

We singled out the association Cyg OB2 which still remains one of the most actively studied objects in the Galaxy (see a history of its investigations in Chentsov et al. 2013). The polarimetric studies of stars in Cyg OB2 have demonstrated a low polarizing efficiency and unusually small values of the maximum polarization wavelength. Therefore, Cyg OB2, marked by a cross in Fig. 3, occupies an isolate position in the lower left corner. It is well known that in this direction the line of sight is aligned along the spiral arm, i.e. we should expect rather small polarization because of a moderate inclination of the magnetic field. From other side, the association Cyg OB2 is rather distant. So, depolarization of stellar radiation may occur due to quite different polarization in several clouds in the line of sight. Taking into account a contribution of foreground polarization seems to lead to an increase of the polarizing efficiency (McMillan & Tapia 1977; Whittet 2015). Evidently, polarization in Cyg OB2 direction needs a further analysis and discussion.

Undoubtedly, it would be interesting to compare the optical polarization of our objects with the submm polarization measured by *Planck*. Unfortunately, the published results were computed at 1° resolution (Planck Collaboration Int. XIX 2015). So, the data can only suggest that this polarization is larger in the region Chamaeleon–Musca than that in Ophiuchus, Taurus and R CrA.

3 MODEL

Our model of interstellar dust grains is exactly the same as used by VH14.² We consider a mixture of silicate and carbonaceous homogeneous spheroids with certain distributions over sizes and orientations, but a fixed ratio a/b , where a and b are the major and minor spheroid semiaxes, respectively. Both the silicate and carbonaceous particles contribute to extinction, but the interstellar polarization is assumed to be produced mainly by silicate particles. This assumption is supported, in particular, by a correlation between the observed interstellar polarization degree and the abundance of silicon in dust grains found in the work of Voshchinnikov et al. (2012). We also suggest that small silicate particles are randomly oriented when their sizes $r_V < r_{V,cut}$, where r_V is the radius of a sphere whose volume is equal to that of the spheroid, $r_V = \sqrt[3]{ab^2}$ for prolate spheroids and $r_V = \sqrt[3]{a^2b}$ for oblate ones.

Let us consider a dust cloud with the uniform magnetic field. The angle between the line of sight and the magnetic field is denoted by Ω ($0^\circ \leq \Omega \leq 90^\circ$). The extinction and linear polarization of unpolarized stellar radiation produced by aligned rotating spheroidal particles are

$$A(\lambda) = 1.086 \sum_j^D \int_0^{r_{V,max,j}} \int_{r_{V,min,j}} \bar{C}_{ext,j}(m_{\lambda,j}, a_j/b_j, r_V, \lambda, \Omega) \times n_j(r_V) dr_V dl, \quad (7)$$

$$P(\lambda) = \int_0^{r_{V,max,Si}} \int_{r_{V,cut,Si}} \bar{C}_{pol,Si}(m_{\lambda,Si}, a_{Si}/b_{Si}, r_V, \lambda, \Omega) \times n_{Si}(r_V) dr_V dl \times 100\%, \quad (8)$$

² In previous modelling (Das et al. 2010, Siebenmorgen et al. 2014) we used other optical constants and grain size distributions.

where

$$\bar{C}_{ext,j} = \left(\frac{2}{\pi}\right)^2 \int_0^{\pi/2} \int_0^{\pi/2} \int_0^{\pi/2} \frac{1}{2} [C_{ext,j}^{TM}(m_{\lambda,j}, \dots, \alpha) + C_{ext,j}^{TE}] \times f_j(\xi, \beta, \dots) d\varphi d\omega d\beta, \quad (9)$$

$$\bar{C}_{pol,Si} = \frac{2}{\pi^2} \int_0^{\pi/2} \int_0^{\pi/2} \int_0^{\pi/2} C_{pol,Si} f_{Si}(\xi, \beta, \dots) \cos 2\psi d\varphi d\omega d\beta, \quad (10)$$

and

$$C_{pol,Si} = \frac{1}{2} [C_{ext,Si}^{TM}(m_{\lambda,Si}, \dots, \alpha) - C_{ext,Si}^{TE}]$$

for prolate spheroids and

$$C_{pol,Si} = C_{ext,Si}^{TE}(m_{\lambda,Si}, \dots, \alpha) - C_{ext,Si}^{TM}$$

for oblate spheroids.

Here D is the distance to the star, λ the wavelength, $m_{\lambda,j}$, a_j/b_j and $n_j(r_V)$ are the refractive index, aspect ratio and size distribution of spheroidal particles of the j th kind ($j = Si$ for silicate particles and $j = C$ for carbonaceous ones, respectively), $r_{V,min,j}$ and $r_{V,max,j}$ are the minimum and maximum radii, respectively, α is the angle between the wave vector of the incident radiation and the rotation axis of a spheroid, and $C_{ext,j}^{TM,TE}$ the extinction cross-sections for two polarization modes connected with the particle orientation relative to the electric vector of the incident radiation (Bohren & Huffman 1983). These cross-sections were calculated using a solution to the light scattering problem for spheroids given by Voshchinnikov & Farafonov (1993). The angle ψ is expressed through $\varphi, \omega, \beta, \Omega$ (see definitions of these angles and relations between them, e.g., in Das et al. 2010, Siebenmorgen et al. 2014), and finally $f_j(\xi, \beta, \dots)$ describes the distribution of the particles of the j th kind over orientations.

We calculate the extinction in the B, V bands as extinction $A(\lambda)$ (see equation 7) averaged over wavelengths within the corresponding passband as follows:

$$A_X = -2.5 \log_{10} \int_{\lambda_1}^{\lambda_2} F_X(\lambda) \exp \left[\frac{A(\lambda)}{1.086} \right] d\lambda, \quad (13)$$

where $F_X(\lambda)$ is the normalized transmittance curve for a band X (=B, V) and λ_1 and λ_2 are the band limits.

When selecting the dust materials, we followed VH14 and choose the amorphous silicate with a 10% volume fraction of Fe ('silicate.FoFe10.RFI') and hydrogen rich aliphatic carbon (a-C:(H) material with a band gap $E_g = 2.5$ eV). The optical constants were taken from Jones et al. (2013) and Jones (2012) for the silicate and carbon, respectively.

An important constituent of the model is the grain size distribution. It is obtained as a result of fitting of the observed interstellar extinction and polarization curves and may be a rather complicated function (see Voshchinnikov 2012 for a review). Here we invoke the results of Hirashita (2012) and Hirashita & Voshchinnikov (2014) who investigated time evolution of the grain size distribution caused by accretion and coagulation in an interstellar cloud. Hirashita & Voshchinnikov (2014) and VH14 examined whether dust grains processed by these mechanisms can explain variations of the interstellar extinction and polarization curves observed in the Milky Way. They assumed that an initial grain size distribution (for time $T = 0$) should fit the mean Milky Way extinction curve

(Weingartner & Draine 2001). It was found that the observational data could be explained provided the model is ‘tuned’, i.e. wh coagulation of silicate dust is more efficient, with the coagulation threshold being removed, and coagulation of carbonaceous dust less efficient compared to the original model. Thus, the time grain processing T is uniquely related to the grain size distribution. VH14 showed that the time scale $T \sim (30-50)(n_{\text{H}}/10^3 \text{cm}^{-3})$ Myr, the polarization maximum shifts to longer wavelengths (λ_{m} grows) and the polarization curve becomes wider (K decreases). growth of K and λ_{max} also occurs, when we increase the cut-size $r_{V,\text{cut}}$ that corresponds to the interface between non-aligned and aligned grains. Both model parameters T and $r_{V,\text{cut}}$ influence the polarizing efficiency $P_{\text{max}}/E(B-V)$ (and P_{max}/A_V) but the degree and direction of grain alignment as well as the particle type and shape may produce similar effects.

Modelling requires a specification of the function describing the distribution of particles over orientations according to a selected alignment mechanism. Two mechanisms are most popular: the magnetic alignment based on the paramagnetic relaxation of grain material containing about one percent of iron impurities (IDG mechanism; Davis & Greenstein 1951), and the radiative torque alignment (RAT alignment) arising from an azimuthal asymmetry of the light scattering by non-spherical particles (Dolginov et al. 1979). Both mechanisms encounter some difficulties.

The DG mechanism requires a stronger magnetic field than the average galactic one, and the polarizing grains were assumed to contain small clusters of iron (Jones & Spitzer 1967) and all needs to be spun up to very high velocities (Purcell 1979).

The RAT mechanism has been updated rather recently (see Draine & Weingartner 1997 and the discussion in Andersson et al. 2015). However, so far, it has been made rather at the qualitative level. The theory of this mechanism is not based on careful light scattering calculations of interstellar polarization as the usage of the Rayleigh reduction factor is appropriate just in the infrared part of spectrum (see, e.g., Whittet et al. 2008). Note also the absence of the correlation between the submillimeter polarization and dust temperature predicted by the RAT mechanism and not detected in *Planck* data (Planck Collaboration XI 2014; Guillet 2015).

Anyway, as the alignment function for the RAT mechanism has not been specified in enough detail (Draine 2015; Andersson et al. 2015), we utilized a properly modified function for the imperfect alignment of the spheroidal grains in Davis–Greenstein mechanism (IDG alignment). In this case, the distribution function $f^{\text{IDG}}(\xi, \beta)$ depends on the orientation parameter ξ and the angle β (Hong & Greenberg 1980). β is the opening angle of the precession cone for the particle angular momentum which precesses around the direction of the magnetic field. The alignment function is written as

$$f^{\text{IDG}}(\xi, \beta) = \frac{\xi \sin \beta}{(\xi^2 \cos^2 \beta + \sin^2 \beta)^{3/2}}. \quad (14)$$

The parameter ξ depends on the particle size r_V , the imaginary part of the magnetic susceptibility of a dust grain $\chi'' = \varkappa \omega_d / T_d$, where ω_d is the angular velocity of the particle, hydrogen number density n_{H} , magnetic field strength B , and temperatures of dust T_d and gas T_{gas} . For particles of the j -th kind,

$$\xi_j^2 = \frac{r_V + \delta_{0,j}^{\text{IDG}}(T_{d,j}/T_{\text{gas}})}{r_V + \delta_{0,j}^{\text{IDG}}}, \quad (15)$$

where

$$\delta_{0,j}^{\text{IDG}} = 8.23 \cdot 10^{23} \frac{\varkappa_j B^2}{n_{\text{H}} T_{\text{gas}}^{1/2} T_{d,j}} \mu\text{m} \quad (16)$$

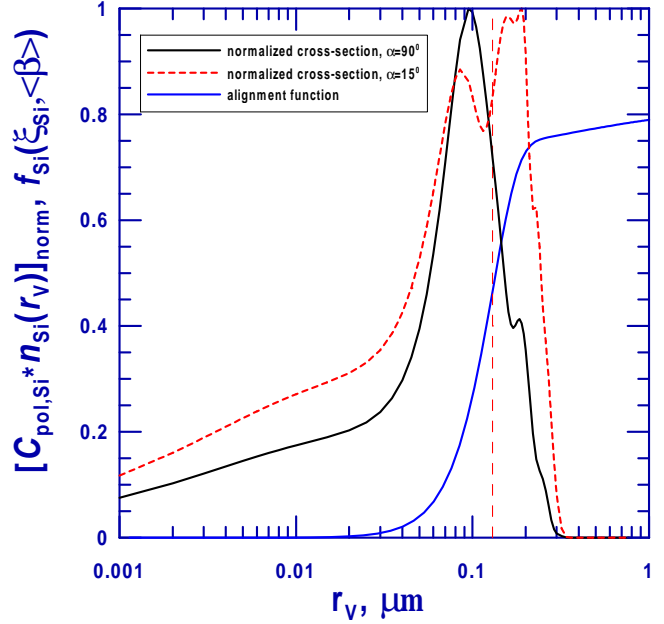


Figure 4. Size dependence of the normalized polarization cross-sections for prolate silicate spheroids with $a/b = 3$ ($\lambda = 0.55 \mu\text{m}$) and the alignment function $f_{\text{Si}}(\xi_{\text{Si}}, \beta)$ for β equal to its average value $\langle \beta \rangle$ ($T = 0$, $r_{V,\text{cut}} = 0.13 \mu\text{m}$, $\delta_{0,\text{Si}}^{\text{IDG}} = 0.5 \mu\text{m}$).

and we assume $T_{\text{gas}} = 10 T_d$. In standard interstellar conditions, we have $\delta_0 \approx 0.3 - 0.5 \mu\text{m}$, which allows one to account for the observed polarization (Das et al. 2010). Note that the DG mechanism produces the ‘‘right’’ alignment when the minor grain axes tend to align parallel to the magnetic field if $T_d < T_{\text{gas}}$. Measurements show that this condition is satisfied even in dense parts of interstellar clouds (Koumpia et al. 2015).

We suggest the following modified IDG alignment function with reduced alignment of small grains (see also Mathis 1986):

$$f_j(\xi_j, \beta, \dots) = [1 - \exp(-r_V/r_{V,\text{cut},j})^3] \times f_j^{\text{IDG}}(\xi_j, \beta), \quad (17)$$

where $r_{V,\text{cut},j}$ is a cut-off parameter. The alignment function (17) gives a smooth switch from non-aligned to aligned grains. It is shown in Fig. 4 for the model with the parameters: $T = 0$ Myr, $r_{V,\text{cut}} = 0.13 \mu\text{m}$ and $\delta_{0,\text{Si}}^{\text{IDG}} = 0.5 \mu\text{m}$ (see Fig. 5). The alignment function was calculated for several grain sizes as a function of the mean precession cone angle $\langle \beta \rangle$ as given by equation (5) in Aannestad & Greenberg (1983). It should be emphasized that our function $f_j(\dots)$ qualitatively agrees with that expected for the RAT mechanism.

Figure 4 also shows the size dependence of the product $C_{\text{pol,Si}}(r_V, \alpha, \dots) n_{\text{Si}}(r_V)$ for $\lambda = 0.55 \mu\text{m}$ normalized to its maximum value. We consider the non-rotating prolate spheroids with $a/b = 3$ in two orientations: $\alpha = 90^\circ$ and 15° . The function $n_{\text{Si}}(r_V)$ corresponds to the initial grain size distribution for time $T = 0$. It is clearly seen that the contribution of larger particles to polarization grows with decreasing the angle α between the wave vector and the particle symmetry axis. The figure demonstrates that a simplified treatment of the partly aligned grains using the Rayleigh reduction factor may be a serious error.

Our model assumes that the magnetic field does not change its direction and strength in the line of sight to the star (within the region where the polarization originates). However, turbulence is known to affect the field. A comparison of our model polarization P with

the observations may require a correction reducing the polarization degree as follows: $P_{\text{corrected}} = FP$. Now one often applies the so called depolarization factor F that depends on the ratio of the regular (uniform) component \mathbf{B}_0 of the magnetic field to the total magnetic field $\mathbf{B}_{\text{tot.}} = \mathbf{B}_0 + \mathbf{B}_t$, where \mathbf{B}_t is turbulent (random) component. Thus, $F = 1$ in the case of the regular magnetic field ($\mathbf{B}_t = 0$) and $F = 0.5$ in the case of the equipartition between the magnetic and turbulent kinetic energy ($\mathbf{B}_t = \mathbf{B}_0$).

4 RESULTS AND DISCUSSION

We have performed calculations of the interstellar extinction and polarization curves for prolate and oblate homogeneous spheroids consisting of silicate and amorphous carbon. The particles of 74 sizes in the range from $r_{V,\text{min}} = 0.001 \mu\text{m}$ to $r_{V,\text{max}} = 1 \mu\text{m}$ with four aspect ratios $a/b = 1.5, 2, 3$ and 4 were utilized. The curves were calculated for 77 wavelengths in the range from $\lambda = 0.2$ to $5 \mu\text{m}$. We computed the colour excess $E(B - V)$, parameter R_V and parameters of the Serkowski curve P_{max} , λ_{max} , and K . The response functions for the B and V bands were taken from Straizys (1992).

In this paper, we focus on a relation between the polarizing efficiency $P_{\text{max}}/E(B - V)$ and λ_{max} . The dependence of the width of the polarization curve (parameter K) on the position of its maximum has been analysed by VH14. It should be emphasized that K and λ_{max} are mainly determined by the size distribution $n_{\text{Si}}(r_V)$ (depending on the time of grain processing T) and the threshold on the size of aligned silicate grains $r_{V,\text{cut}}$. At the same time, K and λ_{max} are weakly affected by the degree (δ_0^{IDG}) and direction (Ω) of the particle orientation. However, it is not the case for the polarizing efficiency. Therefore, we vary the alignment parameters δ_0^{IDG} and Ω (keeping fixed the parameter $\delta_{0,C}^{\text{IDG}} = 0.01 \mu\text{m}$).

Our choice of $P_{\text{max}}/E(B - V)$ as the polarizing efficiency instead of P_{max}/A_V presents the fact that the ratio of the total to selective extinction R_V given by observations is not reliable enough. Furthermore, grain processing in interstellar clouds leads to larger values of R_V (Hirashita & Voshchinnikov 2014; see also Table 3) that produces an additional trend in the behaviour of the ratio P_{max}/A_V (see equation 6) with a growth of T .

We start with a consideration of the model with prolate grains and $a/b = 3$. Variations of the grain type and shape are analysed in Sect. 4.4.

4.1 Dust grains without processing ($T = 0$ Myr)

First, we have calculated the data for diagrams $P_{\text{max}}/E(B - V)$ vs. λ_{max} for the initial size distribution of silicate and carbonaceous grains (Fig. 5). In this case, the average observational Serkowski curve ($\lambda_{\text{max}} = 0.55 \mu\text{m}$, $K = 0.92$) can be fitted if $r_{V,\text{cut}} = 0.13 \mu\text{m}$ (VH14). If we assume $\delta_0^{\text{IDG}} = 0.5 \mu\text{m}$, $\Omega = 60^\circ$, and $F = 1$, the polarizing efficiency of the interstellar medium would achieve $P_{\text{max}}/E(B - V) = 5.23 \text{ \%}/\text{mag}$. (large filled circle in Fig. 5). For $F < 1$, this efficiency drops accordingly.

Figure 5a shows how variations of $r_{V,\text{cut}}$ influence the polarizing efficiency. It is clearly seen that λ_{max} grows and $P_{\text{max}}/E(B - V)$ decreases with a growing cut-off parameter, i.e. for larger values of $r_{V,\text{cut}}$, the polarizing efficiency becomes smaller and the maximum of the curve $P(\lambda)$ shifts to longer wavelengths. This effect is more pronounced for larger values of Ω .

An average size of polarizing dust grains can be found using

the following expression:

$$\langle r_{V,\text{pol, Si}} \rangle = \frac{\int_{r_{V,\text{cut}}}^{r_{V,\text{max}}} r_V n_{\text{Si}}(r_V) dr_V}{\int_{r_{V,\text{cut}}}^{r_{V,\text{max}}} n_{\text{Si}}(r_V) dr_V}. \quad (18)$$

For the model which gives the best approximation to the average observational Serkowski curve ($r_{V,\text{cut}} = 0.13 \mu\text{m}$), $\langle r_{V,\text{pol, Si}} \rangle = 0.17 \mu\text{m}$. For $r_{V,\text{cut}}$ increasing from 0.08 to $0.30 \mu\text{m}$, λ_{max} grows, $P_{\text{max}}/E(B - V)$ reduces and the average grain size $\langle r_{V,\text{pol, Si}} \rangle$ increases from 0.12 to $0.31 \mu\text{m}$.

Note that for the models with $r_{V,\text{cut}} \lesssim 0.12 \mu\text{m}$ the polarization peaks in the blue part of spectrum ($\lambda_{\text{max}} \lesssim 0.5 \mu\text{m}$) that is outside the range of the observational values of λ_{max} except for the case of Cyg OB2 (Fig. 5a). The models with $r_{V,\text{cut}} > 0.12 \mu\text{m}$ can explain only a small part of the observational data if we fix the parameter δ_0^{IDG} . Also it is evident that the cut-off parameter should not exceed $\sim 0.2 - 0.3 \mu\text{m}$.

By increasing the degree of grain alignment and the angle Ω it is possible to reproduce almost all observations of open clusters (Fig. 5b). However, the models do not give polarization curves with $\lambda_{\text{max}} \gtrsim 0.65 \mu\text{m}$ observed in several dust clouds. In this case, even very large values of δ_0^{IDG} would not do.

Summarizing, we can conclude that the models with the initial size distribution of unprocessed dust grains *fail* to explain the observational data with large values of λ_{max} .

4.2 Processed dust grains ($T = 10 - 40$ Myr)

Next we investigate changes of the polarizing efficiency owing to evolution of the grain size distribution. Our results are shown in Fig. 6 for the tuned models (see Hirashita & Voshchinnikov 2014). The left panel illustrates the combined effects of $r_{V,\text{cut}}$ and Ω variations for the model with $T = 20$ Myr.³ In this case, we have obtained the polarization curve that is most close to the average observational Serkowski one when $r_{V,\text{cut}} = 0.095 \mu\text{m}$, $\langle r_{V,\text{pol, Si}} \rangle = 0.15 \mu\text{m}$ ($F = 1$). From a comparison of Figs. 6a and 5a, it is clearly seen that the evolutionary effects are very important: by varying $r_{V,\text{cut}}$ and Ω in the model with $T = 20$ Myr it is possible, in fact, to explain *all* observational data both for open clusters and dark clouds when $F = 1$, and all except for two largest values when $F = 0.5$. If we assume $\delta_0^{\text{IDG}} = 0.5 \mu\text{m}$, the models with the cut-off $0.08 \mu\text{m} \lesssim r_{V,\text{cut}} \lesssim 0.2 \mu\text{m}$ and $\Omega \gtrsim 30^\circ$ give the polarizing efficiency and λ_{max} similar to the observed average values when $F < 0.8$.

Note that an explanation of the available observational data does not require the models with more processed dust grains ($T \gtrsim 30$ Myr). This follows from Fig. 6b where we present the models with increasing time of grain evolution and fixed other parameters. With growing T both the polarizing efficiency and the wavelength of maximum polarization grow, and this effect is more pronounced if the direction of the magnetic field is perpendicular to the line of sight (i.e. for $\Omega = 90^\circ$).

³ This time of dust processing in a molecular cloud with the hydrogen density $n_{\text{H}} = 10^3 \text{ cm}^{-3}$ (Hirashita & Voshchinnikov 2014).

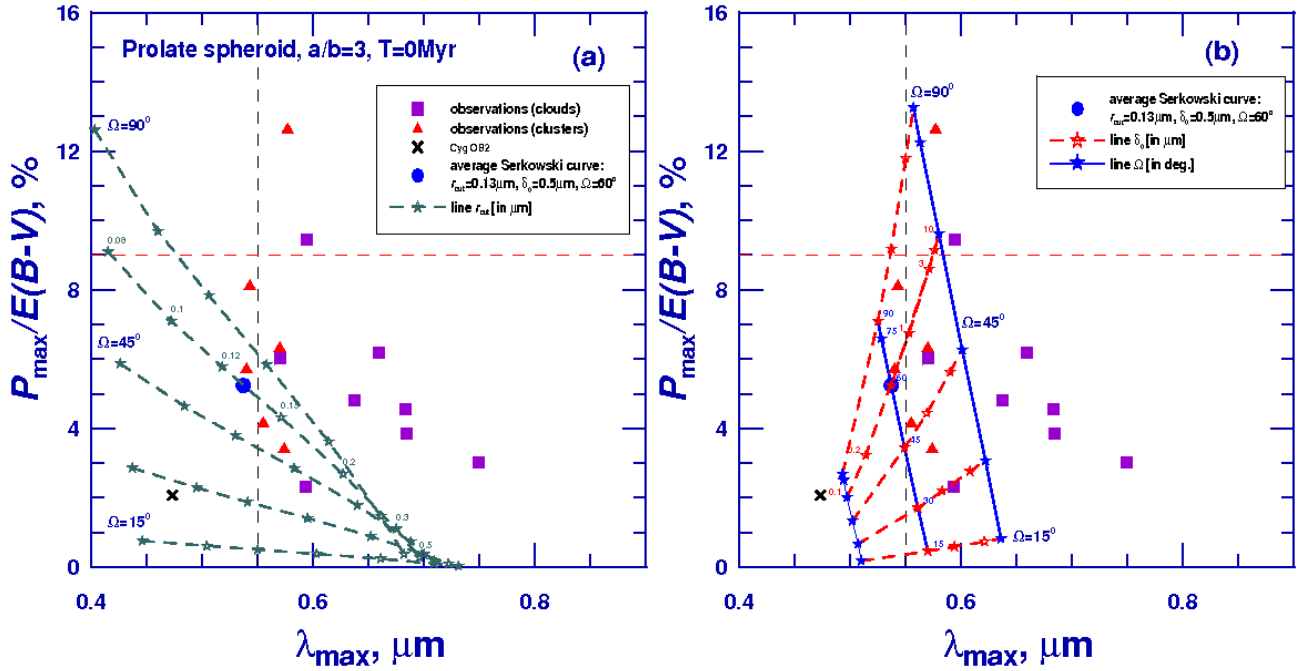


Figure 5. Polarizing efficiency $P_{\max}/E(B-V)$ versus the wavelength of maximum polarization λ_{\max} . Symbols (filled squares and triangles and cross) show the average values for clouds and clusters presented in Table 1 (columns 7 and 8) and Fig. 3. Vertical and horizontal dashed lines correspond to the mean interstellar value of $\lambda_{\max} = 0.55 \mu\text{m}$ and the upper limit of the polarizing efficiency given by equation (5). Stars (*) connected with solid and dashed lines show theoretical results calculated for the model: prolate spheroids, $a/b = 3$. Large filled circle corresponds to the model with parameters: $T = 0 \text{ Myr}$, $r_{V,\text{cut}} = 0.13 \mu\text{m}$, $\delta_{0,\text{Si}}^{\text{IDG}} = 0.5 \mu\text{m}$, $\Omega = 60^\circ$ which is the closest to the average observational Serkowski curve ($\lambda_{\max} = 0.55 \mu\text{m}$, $K = 0.92$). Panels (a) and (b) illustrate the variations of the cut-off parameter $r_{V,\text{cut}}$ and the degree ($\delta_{0,\text{Si}}^{\text{IDG}}$) and direction (Ω) of grain alignment, respectively. The depolarization factor F can be involved by a proper vertical shift of the theoretical curves.

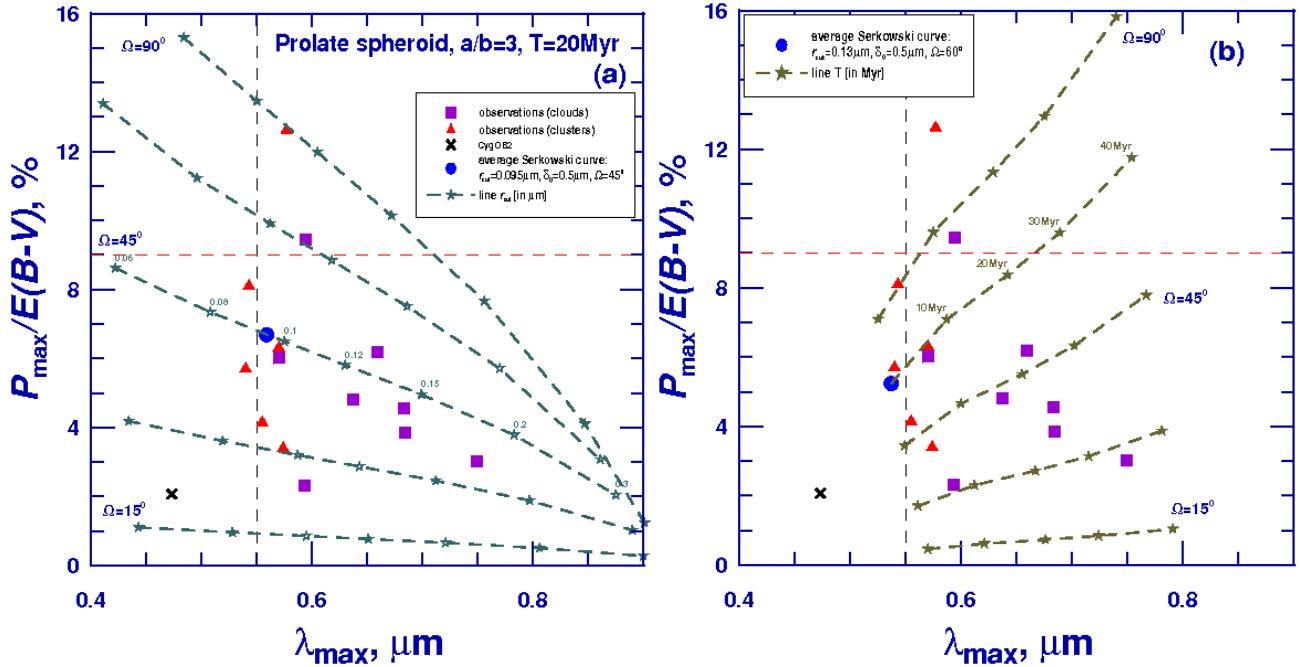


Figure 6. The same as in Fig. 5 but now for the models with different time of grain evolution T . Panel (a) illustrates the variations the cut-off parameter $r_{V,\text{cut}}$ for the model with prolate spheroids, $a/b = 3$, $T = 20 \text{ Myr}$, $\delta_{0,\text{Si}}^{\text{IDG}} = 0.5 \mu\text{m}$. Large filled circle corresponds to the model with $r_{V,\text{cut}} = 0.095 \mu\text{m}$ and $\Omega = 45^\circ$. Panel (b) illustrates the variations of the time of grain evolution for the model with parameters: $r_{V,\text{cut}} = 0.13 \mu\text{m}$, $\delta_{0,\text{Si}}^{\text{IDG}} = 0.5 \mu\text{m}$, $\Omega = 60^\circ$.

Table 2. Changes of the observed characteristics in dependence on the model parameters.

Parameter	$P_{\max}/E(B-V)$	λ_{\max}	K	R_V
$r_{V,\text{cut,Si}}$ ↗	↘	↗	↗	0
T ↗	↗	↗	↘	↗
$\delta_{0,\text{Si}}^{\text{IDG}}$ ↗	↗	↗	0	0
Ω ↗	↗	↘	0	0
prolate → oblate	↗	↗	↗	↘
a/b (prolate) ↗	↗	↘	↘	↘
a/b (oblate) ↗	↗	0	↗	↘

Note: ↗ or ↘ indicate the increase or decrease of the corresponding quantity with the growth of parameter. 0 means a little change of the quantity.

Parameters: $r_{V,\text{cut,Si}}$ – minimum size of polarizing Si grains; T – time of grain processing; $\delta_{0,\text{Si}}^{\text{IDG}}$ – degree of grain alignment; Ω – direction of magnetic field.

4.3 Models with prolate grains and $a/b = 3$: summary

Here we discuss the models in the context of simultaneous variations of the four model parameters: $r_{V,\text{cut,Si}}$, T , $\delta_{0,\text{Si}}^{\text{IDG}}$ and Ω . The first two parameters affect the size of polarizing and processed grains, the last two parameters determine the degree and direction of grain alignment. The type and shape of the particles (prolate spheroids with $a/b = 3$) remain the same in all the models.

If we assume that the polarizing efficiency on average is $P_{\max}/E(B-V) = 4 - 6\%$, the average observational Serkowski curve can be reproduced by the models with $\Omega = 60^\circ$ ($T = 0$ Myr) and $\Omega = 45^\circ$ ($T = 20$ Myr) for $F = 1$. These models are plotted by large filled circles in the left and right panels of Fig. 7, respectively. Using the circles as starting points, we have calculated a set of models with reasonable variations of the four mentioned parameters. The final picture thus obtained resembles an *octopus* shown in Fig. 7 where just one model parameter varies along each line. A distinguishing feature of the Figure is the different behaviour of these four lines, which allows one to estimate the effects of changes of the parameters or their combination. Evidently, the additional information about the width of the polarization curve (the parameter K of the Serkowski curve) would be helpful. Variations of the observed polarization with changes of the model parameters show the trends summarized in Table 2. For $F < 1$, the octopus moves to the bottom accordingly.

Figure 7a demonstrates that the models with unprocessed dust grains ($T = 0$ Myr) cannot explain the observational points in the right and upper parts of the plots $P_{\max}/E(B-V)$ vs λ_{\max} . The models with a higher value of the alignment parameter $\delta_{0,\text{Si}}^{\text{IDG}}$ do not solve the problem. Thus, we need to consider the models with larger dust grains resulting from dust evolution in molecular clouds (see Fig. 7b). As follows from this figure, the models with $T = 20$ Myr permit to reproduce the average observational data for clouds and clusters under consideration if we vary three additional parameters: $r_{V,\text{cut,Si}}$, $\delta_{0,\text{Si}}^{\text{IDG}}$ and Ω . This fact illustrates the models plotted by dot-dashed lines in Fig. 7b for $\delta_{0,\text{Si}}^{\text{IDG}} = 1.0 \mu\text{m}$ and two values of the depolarization factor F . The upper curve shows the results in the case of the regular magnetic field ($F = 1$) while the lower curve is obtained for the model that takes into account the turbulent component of the magnetic field ($F = 0.5$).

A detailed analysis of observational data for separate objects must be made more carefully involving information on interstellar extinction and will be carried out in the next paper.

4.4 Variations of grain type and shape

The interstellar polarization is often stated to provide information about the shape of cosmic dust grains (see, e.g., Whittet 2003). So far such modelling has been made for infinite circular cylinders and spheroids (see Voshchinnikov 2012 for a review). The infinite cylinders are the simplest non-spherical particles whose shape cannot be varied. The spheroids were considered just in a few papers. In particular, Rogers & Martin (1979) and Kim & Martin (1995) used prolate and oblate spheroidal grains with different aspect ratios a/b . But their consideration was restricted by perfectly aligned rotating/non-rotating particles with a fixed orientation of the magnetic field relative to the line of sight 90° . However, in this case the polarizing efficiency should be in several times larger than the observed maximum even for $F = 0.5$.

We have calculated the interstellar extinction and polarization for prolate and oblate spheroids with four aspect ratios $a/b = 1.5, 2, 3$ and 4. Some of these results are given in Fig. 8 and Table 3 for $r_{V,\text{cut}} = 0.1, 0.2 \mu\text{m}$ and $T = 0, 20$ Myr. Comparing Fig. 8 with Fig. 7 we can arrive to the conclusion that for prolate spheroids variations of the aspect ratio seem to be less important than variations of other model parameters, namely $r_{V,\text{cut,Si}}$, T , $\delta_{0,\text{Si}}^{\text{IDG}}$ and Ω . When the parameter a/b grows, λ_{\max} reduces for prolate spheroids but remains almost the same for oblate spheroids. Note also that the oblate particles are more efficient polarizers and can easily explain extremely large values of the polarizing efficiency observed, for example, in Musca (Fig. 8a) when $F \sim 0.8$.

A difference between prolate and oblate spheroids also appears in the shape of the polarization curve: a growth of the parameter a/b makes the curve wider (K reduces) for prolate particles and narrower (K increases) for oblate particles (Table 3).⁴ VH14 compiled the parameters of Serkowski curve for a sample of 160 lines of sight and found the observational limits: $K \approx 0.5 - 1.5$ and $\lambda_{\max} \approx 0.35 - 0.8 \mu\text{m}$. As follows from Table 3, the major part of the models with oblate particles is beyond these limits.

A more detailed consideration of the shape effects is outside the scope of this work and requires a further investigation.

4.5 General discussion

It is evident that any modelling allows determining just of intervals for the model parameter values. Nevertheless, it provides some trends in the behaviour of the observed characteristics (Table 2). Using the diagrams $P_{\max}/E(B-V)$ vs. λ_{\max} (Figs. 5 – 8) and K vs. λ_{\max} (VH14) we can conclude that our model has two key parameters: the threshold on the size of aligned silicate grains $r_{V,\text{cut,Si}}$ and time of grain processing T . After comparing with observations, it is possible to restrict the parameters: $0.05 \mu\text{m} \lesssim r_{V,\text{cut,Si}} \lesssim 0.2 \mu\text{m}$ and $T \lesssim 20 - 30$ Myr.⁵ Note that a growth of T is accompanied by an increase of the total to selective extinction ratio R_V (Hirashita & Voshchinnikov 2014; Table 3). Variations of the key parameters would explain the general observational trends while additional polarization details could be reproduced if we changed degree and direction of grain alignment $\delta_{0,\text{Si}}^{\text{IDG}}$ and Ω . Calculations show that we can hardly distinguish the

⁴ These tendencies are noticed in Table 2.

⁵ This time does not contradict to the lifetime of molecular clouds (Pagani et al. 2011; Dobbs & Pringle 2013) because the time-scales of accretion and coagulation $\propto n_{\text{H}}^{-1}$ (Hirashita & Voshchinnikov 2014), i.e. if we adopt $n_{\text{H}} = 10^4 \text{ cm}^{-3}$ instead of 10^3 cm^{-3} , the same size distributions are reached at one-tenth the time.

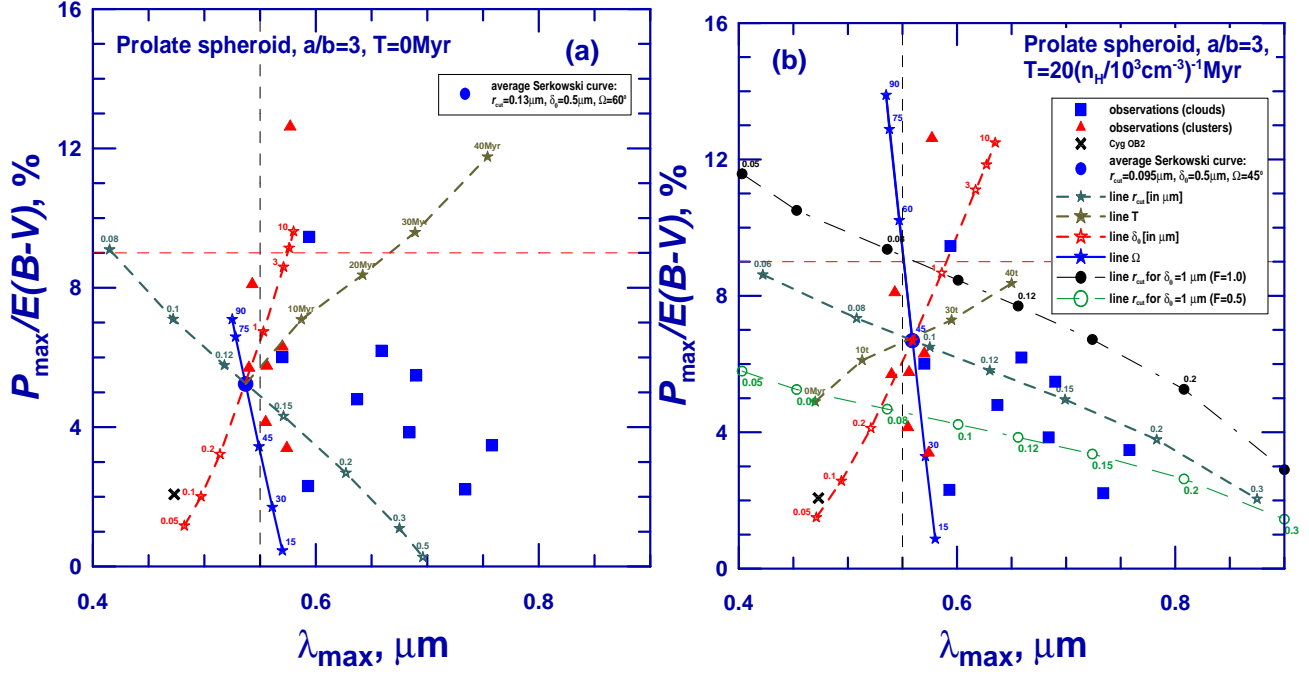


Figure 7. Polarizing efficiency $P_{\max}/E(B-V)$ versus the wavelength of maximum polarization λ_{\max} . Symbols show the observational data presented in Table 1 (columns 7 and 8) and Fig. 3. Stars (\star) connected with solid and dashed lines illustrate theoretical results calculated for the model: prolate spheroids, $a/b = 3$, $T = 0$ Myr (a) and $T = 20$ Myr (b). Large filled circles correspond to the models closest to the average observational Serkowski curve (see Fig. 5). Circles connected with dot-dashed lines illustrate theoretical results calculated for the models with $T = 20$ Myr and the depolarization factors $F = 1$ (filled circles) and $F = 0.5$ (open circles). Panels illustrate the variations of the different model parameters.

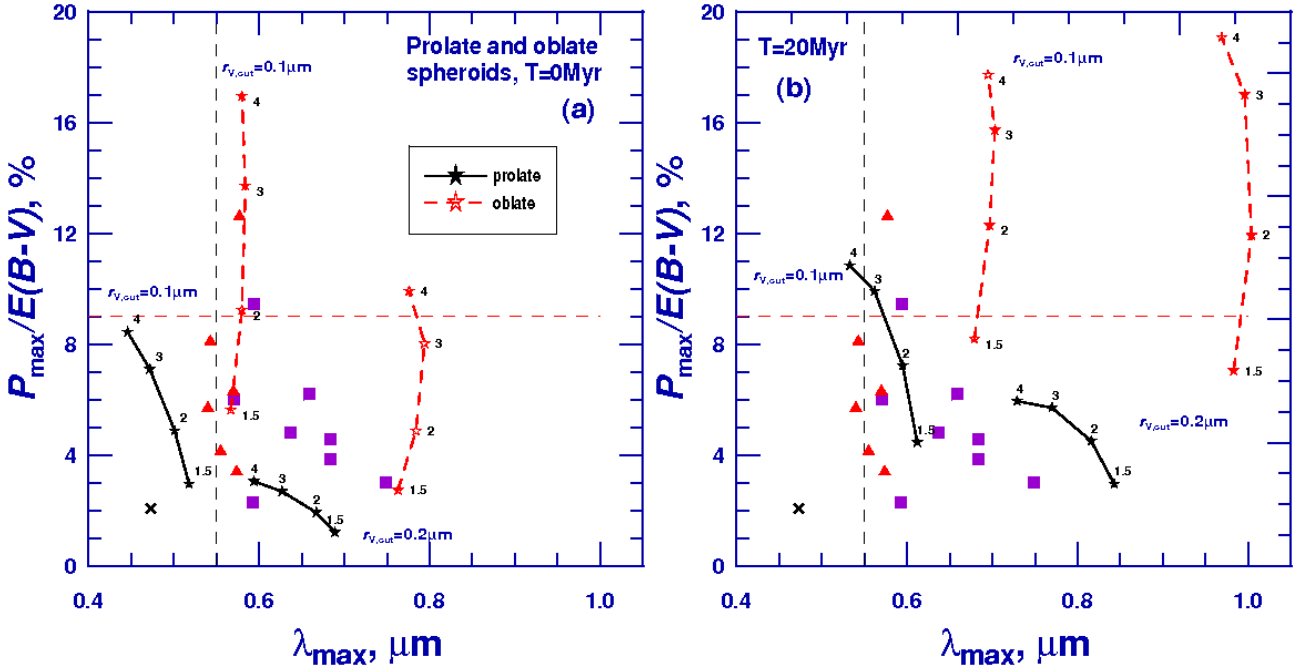


Figure 8. Polarizing efficiency $P_{\max}/E(B-V)$ versus the wavelength of maximum polarization λ_{\max} . Symbols show the observational data presented in Table 1 (columns 7 and 8) and Fig. 3. Stars (\star) connected with solid and dashed lines demonstrate theoretical results calculated for the model: $\delta_{0, \text{Si}}^{\text{DG}} = 0.5 \mu\text{m}$, $\Omega = 60^\circ$, $T = 0$ Myr (a) and $T = 20$ Myr (b). Panels illustrate the variations of the particle type (prolate/oblate) and particle shape (aspect ratio a/b). The values of the parameters $r_{V, \text{cut}}$ and a/b are indicated.

Table 3. Observed characteristics in dependence on the particle shape and time of grain processing T (the model with $\delta_{0,\text{Si}}^{\text{IDG}} = 0.5 \mu\text{m}$, $\Omega = 60^\circ$).

a/b	$T = 0 \text{ Myr}$				$T = 20 \text{ Myr}$			
	$P_{\text{max}}/E(B-V)$	λ_{max}	K	R_V	$P_{\text{max}}/E(B-V)$	λ_{max}	K	R_V
	Prolate spheroid, $r_{V,\text{cut}} = 0.1 \mu\text{m}$				Prolate spheroid, $r_{V,\text{cut}} = 0.1 \mu\text{m}$			
1.5	2.96	0.518	1.135	3.633	4.46	0.612	1.013	6.060
2.0	4.88	0.501	1.073	3.580	7.23	0.595	0.969	5.971
3.0	7.10	0.472	0.983	3.397	9.91	0.562	0.904	5.534
4.0	8.44	0.446	0.925	3.218	10.84	0.533	0.861	5.045
	Prolate spheroid, $r_{V,\text{cut}} = 0.2 \mu\text{m}$				Prolate spheroid, $r_{V,\text{cut}} = 0.2 \mu\text{m}$			
1.5	1.21	0.689	1.370		2.956	0.843	1.326	
2.0	1.93	0.667	1.282		4.506	0.816	1.246	
3.0	2.68	0.627	1.161		5.708	0.770	1.136	
4.0	3.05	0.594	1.088		5.947	0.729	1.070	
	Oblate spheroid, $r_{V,\text{cut}} = 0.1 \mu\text{m}$				Oblate spheroid, $r_{V,\text{cut}} = 0.1 \mu\text{m}$			
1.5	5.62	0.567	1.357	3.495	8.18	0.679	1.050	5.708
2.0	9.23	0.580	1.442	3.384	12.29	0.697	1.107	5.146
3.0	13.72	0.584	1.524	3.197	15.73	0.703	1.194	4.266
4.0	16.95	0.580	1.681	3.109	17.72	0.695	1.306	3.822
	Oblate spheroid, $r_{V,\text{cut}} = 0.2 \mu\text{m}$				Oblate spheroid, $r_{V,\text{cut}} = 0.2 \mu\text{m}$			
1.5	2.73	0.763	1.700		7.05	0.983	1.297	
2.0	4.87	0.784	1.877		11.93	1.004	1.489	
3.0	8.02	0.794	2.035		17.01	0.996	1.820	
4.0	9.91	0.776	2.242		19.07	0.969	1.992	

cases when the direction of the magnetic field is near the line of sight ($\Omega \lesssim 15^\circ$) or close to perpendicular to the line of sight ($\Omega = 75^\circ - 90^\circ$). A distinction of the degree of grain alignment also presents a problem if $\delta_{0,\text{Si}}^{\text{IDG}} \gtrsim 3 - 5 \mu\text{m}$.

The overall picture of variations of the polarizing efficiency presented above would not dramatically change if we varied the aspect ratio a/b of prolate grains (Fig. 8, Table 3). Thus determining the shape of the particles like ‘cigars’ would be problematic.

The polarizing efficiency for oblate particles significantly exceeds that of prolate ones. Thus, it is possible to reduce the alignment degree or particle aspect ratio. However, very flattened ‘pancakes’ ($a/b \gtrsim 3$) must be ruled out because they produce too narrow polarization curves.

5 CONCLUSIONS

The main results of the paper can be formulated as follows:

(i) We collected the observational data about the polarizing efficiency $P_{\text{max}}/E(B-V)$ and the position of the maximum polarization λ_{max} for 243 stars in 17 objects separated into two groups: dark clouds and open clusters. The average data for these two groups are distinguished by the parameter λ_{max} . For open clusters, the mean values of λ_{max} are grouped around the average interstellar value $0.55 \mu\text{m}$ with rather small deviations. For dark clouds, the values of $\langle \lambda_{\text{max}} \rangle$ may be significantly larger than $0.55 \mu\text{m}$ and have a wide scattering.

(ii) We utilized the model applied earlier by Voshchinnikov & Hirashita (2014) and including time evolution of the grain size distribution due to the accretion and coagulation processes and new optical constants of grain materials. To calculate the polarization curves, we used homogeneous silicate and carbonaceous spheroidal particles of different aspect ratios a/b having imperfect alignment. It was assumed that polarization was mainly produced by large silicate particles with sizes $r_V \gtrsim r_{V,\text{cut}}$.

We calculated the wavelength dependence of extinction and polarization and determined the parameters $P_{\text{max}}/E(B-V)$ and λ_{max} .

(iii) We focused on the interpretation of the observed relation between $P_{\text{max}}/E(B-V)$ and λ_{max} keeping in mind probable depolarization effect caused by the random component of the magnetic field. Theoretically both quantities are mainly determined by two key parameters: the threshold on the size of aligned silicate grains $r_{V,\text{cut}}$ and time of grain processing T . We found that the models with the initial size distribution (no grain processing, $T = 0 \text{ Myr}$) that reproduce the average curve of the interstellar extinction fail to explain the data with $\lambda_{\text{max}} \gtrsim 0.65 \mu\text{m}$ observed in several dark clouds. An inclusion of evolutionary effects allows us to find the models which give the polarizing efficiency and λ_{max} values similar to the average observed ones for reasonable depolarization ($F \sim 0.5 - 0.8$). This occurs for $0.05 \mu\text{m} \lesssim r_{V,\text{cut,Si}} \lesssim 0.2 \mu\text{m}$ and $T \lesssim (20 - 30)(n_{\text{H}}/10^3 \text{ cm}^{-3})^{-1} \text{ Myr}$ and is in agreement with the lifetime of molecular clouds. The additional polarization details are reproduced if we change the degree (δ_0^{IDG}) and direction (Ω) of particle orientation. However, these results cannot yet be a conclusive evidence that the dust evolution only can completely explain the observational data under consideration because of a rather large number of the parameters still involved in our modeling. A more detailed analysis in particular that involving the width of the polarization curve is required.

(iv) We found that generally the change of the aspect ratio a/b of prolate grains would not dramatically influence the variations of the polarizing efficiency that makes the determination of the grain shape rather problematic for prolate particles. The polarizing efficiency for oblate spheroids significantly exceeds that of prolate ones but particles with $a/b \gtrsim 3$ must be excluded because they produce too narrow polarization curves that are not observed.

ACKNOWLEDGMENTS

We are grateful to anonymous referee for very useful comments and suggestions and thank A. P. Jones for sending us the refractive indexes in the tabular form and interesting discussions. We acknowledge the support from RFBR grant 16-02-00194 and RFBR–DST grant 16-52-45005.

REFERENCES

- Aannestad P. A., & Greenberg J. M., 1983, *ApJ*, 272, 551
 Andersson B. - G., & Potter S. B., 2007, *ApJ*, 665, 369
 Andersson B. - G., Lazarian A. & Vaillancourt J. E., 2015, *ARAA*, 53, 501
 Bohren C. F., Huffman D. R., 1983, *Absorption and Scattering of Light by Small Particles*, Wiley, New York
 Chentsov E. L., Klochkova V. G., Panchuk V. E., Yuskin M. V., & Nasonov D. S., 2013, *Astron. Rep.*, 57, 527
 Coyne G. V., Tapia S., & Vrba F. J., 1979, *AJ*, 84, 356
 Das H. K., Voshchinnikov N. V., & Il'in V. B., 2010, *MNRAS*, 404, 265
 Davis L., & Greenstein J.L. 1951, *ApJ*, 114, 206
 Dobbs C. L., & Pringle J. E., 2012, *MNRAS*, 432, 653
 Dolginov A. Z., Gnedin Yu. N., & Silant'ev N. A., 1979, *Propagation and Polarization of Radiation in Cosmic Medium*, Moscow, Nauka
 Draine B. T., 2015, Report on IAU FM5, Aug. 12
 Draine, B. T., & Weingartner, J. C., 1997, *ApJ*, 480, 663
 Efimov Yu. S., 2009, *Bull. CrAO*, 105, 126
 Guillet V., 2015, Dr. habil. thesis, Université Paris-Sud 11
 Hirashita H., 2012, *MNRAS*, 422, 1263
 Hirashita H., & Voshchinnikov N. V., 2014, *MNRAS*, 437, 1636
 Hong S. S., & Greenberg J. M., 1980, *A&A*, 88, 194
 Hsu J., 1985, PhD thesis, University of Texas, Austin
 Jones A. P., 2012, *A&A*, 540, A2 (corrigendum 2012, *A&A*, 545, C2)
 Jones A. P., Fanciullo L., Köhler M., Verstraete L., Guillet V., Boccio M., & Ysard N., 2013, *A&A*, 558, A62
 Jones R. V. & Spitzer L. 1967, *ApJ*, 147, 943
 Jones T. J., Klebe D., Dickey J.M., 1992, *ApJ*, 389, 602
 Kim S. - H., & Martin P. G., 1995, *ApJ*, 444, 293
 Knude J., 2010, arXiv: 1006.3676
 Koumpia E., Harvey P.M., Ossenkopf V., van der Tak F.F.S., Mookerjee B., Fuente A., & Kramer C., 2015, *A&A*, 580, A68
 Lallement, R., Vergely, J. - L., Valette, B., Puspitarini, L., Eyer, L., & Casagrande, L., 2014, *A&A*, 561, A91
 Martin, P. G., Adamson, A. J., Whittet, D. C. B., Hough, J. H., Bailey, J. A., Kim, S. - H., Sato, S., Tamura, M., & Yamashita, T., 1992, *ApJ*, 392, 691
 Mathis, J. S., 1986, *ApJ*, 308, 281
 McGregor P. J., Harrison, T. E., Hough, J. H., & Bailey, J. A., 1994, *MNRAS*, 267, 755
 McMillan R., S., & Tapia, S., 1977, *ApJ*, 212, 714
 Medhi B., J., Maheswar, G., Brijesh, K., Pandey, J. C., Kumar, T. S., & Sagar, R., 2007, *MNRAS*, 378, 881
 Medhi B., J., Maheswar, G., Pandey, J. C., Kumar, T. S., & Sagar, R., 2008, *MNRAS*, 388, 105
 Messenger D. W., Whittet D. C. B., & Roberge W. G., 1997, *ApJ*, 487, 319
 Myers P. C., & Goodman A. A., 1991, *ApJ*, 373, 509
 Pagani, L., Roueff, E., & Lesafre, P., 2011, *ApJ*, 739, L35
 Planck 2013 results XI, 2014, *A&A*, 571, A11
 Planck intermediate results XIX, 2015, *A&A*, 576, A104
 Planck intermediate results XXXII, 2016, *A&A*, 586, A135
 Planck intermediate results XXXV, 2016, *A&A*, 586, A138
 Planck intermediate results XLIV, 2016, arXiv:1604.01029
 Purcell E. M., 1979, *ApJ*, 231, 404
 Rogers, C., & Martin, P. G., 1979, *ApJ*, 228, 450
 Serkowski K., 1973, in: Greenberg J. M., Hayes D. S., eds, Proc. IAU Symp 52, *Interstellar Dust and Related Topics*, Reidel, Dordrecht, p. 145
 Serkowski, K., Mathewson, D. S., & Ford, V. L., 1975, *ApJ*, 196, 261
 Siebenmorgen, R., Voshchinnikov, N. V., & Bagnulo, S., 2014, *A&A*, 561, A82
 Snow, T. P., Destree, J. D., & Welty, D. E., 2008, *ApJ*, 679, 512
 Strazys, V., 1992, *Multicolor Stellar Photometry*, Pachart Publ. House, Tucson
 Vergne, M. M., Feinstein, C., Martínez, R., Orsatti, A. M., & Alvarez, M. P., 2010, *MNRAS*, 403, 2041
 Voshchinnikov, N. V., 2012, *J. Quant. Spectrosc. Radiative Transfer*, 113, 2334
 Voshchinnikov, N. V., & Das, H. K., 2008, *J. Quant. Spectrosc. Radiative Transfer*, 109, 1527
 Voshchinnikov, N. V., & Farafonov, V. G., 1993, *Ap&SS*, 204, 19
 Voshchinnikov, N. V., & Hirashita, H., 2014, *MNRAS*, 445, 301 (VH14)
 Voshchinnikov, N. V., Das, H. K., Yakovlev, I. S., & Il'in, V. B., 2013, *Astron. Let.*, 39, 421
 Voshchinnikov, N. V., Henning, Th., Prokopenko, M. S., & Das, H. K., 2012, *A&A*, 541, A52
 Vrba, F. J., Baierlein, L., & Herbst, W., 1987, *ApJ*, 317, 207
 Vrba, F. J., Coyne, G. V., & Tapia, S., 1981, *ApJ*, 243, 489
 Vrba, F. J., Coyne, G. V., & Tapia, S., 1993, *AJ*, 105, 1010
 Weingartner, J. C., & Draine, B. T., 2001, *ApJ*, 548, 296
 Whittet, D. C. B., 2003, *Dust in the Galactic Environments*. 2nd ed., IOP Publishing, Bristol
 Whittet, D. C. B., 2015, *ApJ*, 811, 110
 Whittet, D. C. B., Gerakines, P. A., Hough, J. H., & Shenoy, S. S., 2001, *ApJ*, 547, 872
 Whittet, D. C. B., Hough, J. H., Lazarian, A., & Hoang, T., 2008, *ApJ*, 674, 304
 Whittet, D. C. B., Martin, P. G., Hough, J. H., Rouse, M. F., Bailey, J. A., & Axon, D. J., 1992, *ApJ*, 386, 562
 Wilking, B. A., Lebofsky, M. J. & Rieke, G. H., 1982, *AJ*, 87, 695

This paper has been typeset from a $\text{\TeX}/\text{\LaTeX}$ file prepared by the author.